Sliding Mode Control of an MRI-Compatible Pneumatically Actuated Robot

David B. Comber, Diana Cardona, Robert J. Webster, III, Eric J. Barth
Department of Mechanical Engineering, Vanderbilt University

ABSTRACT

Magnetically sensitive environments such as MRI scanners preclude the use of traditional electromagnetic actuators. Pneumatic piston-cylinders are well-suited actuators for MRI-guided robots, but the nonlinear dynamics of the working fluid creates a challenging controls problem. Precision control of the actuators is needed for the robot to achieve high targeting accuracy. This paper reports a five degree-of-freedom MRI-compatible robot and a sliding mode controller for high-accuracy position tracking. Mean steady-state errors for needle translation and rotation in free space are 0.006 mm and 0.3 degrees, respectively.

1 INTRODUCTION

One of the world's oldest recognized diseases, epilepsy affects more than 50 million patients globally (1). In as many as 30 percent of cases, anticonvulsant medications fail to provide seizure control and the patient is left at risk for sudden unexplained death in epilepsy (1). For these patients, surgical resection of the hippocampus, where seizures commonly begin, is a potentially permanent cure, yet the rate of undertreatment exceeds 50 percent in several developed nations (2-4). Hence, there is a compelling case to develop a minimally invasive alternative to surgery.

There are several motivations for a procedure of this kind to use real-time MRI guidance. This technology can provide high-quality images to locate the tip of a needle in soft tissue, and MRI can be used to monitor the delivery of thermal therapy through MR thermometry. However, the closed bore of the MRI scanner limits access to the patient such that a surgical robot is essentially required to do the procedure.

Because traditional electromagnetic actuators are not MRI-compatible, MRI-guided robots have generally used one of two forms of actuation: piezoelectric or fluid power. It has been demonstrated that pneumatic piston-cylinders do not reduce the signal-to-noise ratio (SNR) of the scanner, while piezoelectric motors have a moderate to severe impact (5). Like pneumatics, hydraulic actuators also can be fully compatible because the fundamental principles of actuation are free from electronics.

For surgical applications, pneumatic actuation has several key advantages over hydraulics. In the event of a system leak, hydraulic fluid creates a mess, even if the fluid is sterile, and these leaks can pose a safety hazard to the patient or clinicians. Furthermore, because standard hydraulic fluids are not sterilizable, water or saline is typically used. These fluids can cause system corrosion, and their poor lubrication properties can lead to stick-slip behavior.

In selecting a type of actuation, it is important to also consider how easily the surgical robot can integrate with existing operating rooms. The gas supply for pneumatic robots can come directly from the nitrogen tanks or instrument air supplies that are already available in hospitals. Thus, while hydraulic robots require an auxiliary supply system, pneumatic robots can easily integrate into existing hospital facilities.

Despite the nonlinearities of compressible gas dynamics, high precision control for pneumatics is feasible and has been demonstrated to sub-millimeter accuracy for MRI-compatible piston-cylinders (6). In needle tip placement experiments, a pneumatic robot for prostate brachytherapy has achieved 0.94 mm rms error (7). This paper reports a 5-dof pneumatic robot design for the treatment of epilepsy by hyperthermal ablation. The design and implementation of a sliding mode controller is described. The accuracies in free space for the robot mechanisms approach the resolution of the encoders.

2 MECHANICAL DESIGN

There are several challenging constraints on the design of a surgical robot for intraoperative MRI use. Its dimensions are limited by the bore diameter of the scanner, the allowable materials for parts are restricted to plastics and small amounts of non-magnetic metals, and most electronics must be remotely located several meters away from the scanner. Additionally, the mechanisms must be low friction to allow for precision control of the actuators.

Using these design objectives, a five degree-of-freedom prototype has been designed and manufactured. It is designed to steer an active cannula, a type of continuum robot capable of curving around critical structures in the brain. This needle is made up of three concentric tubes as shown in Fig. 1. An outer, straight titanium tube reaches from the back of the skull to the tail of the hippocampus. The middle and inner tubes are superelastic nitinol. The middle tube is pre-curved to fit the desired needle trajectory for ablation. Thus it requires two degrees of freedom, translation and rotation. Likewise, the innermost nitinol tube is designed to translate and rotate the ablator with a catheter, thus delivering the thermal therapy. In Fig. 1, the active cannula is shown delivering the ablator to the hippocampus, which was modeled in CAD from sagittal and horizontal photographs of a dissected hippocampus.

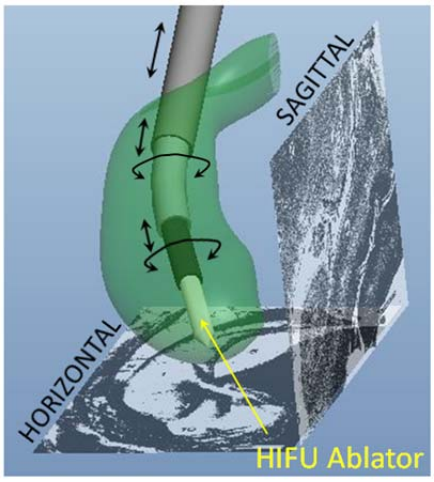

Figure 1: Degrees of freedom for active cannula to deliver ablator to hippocampus

2.1 Mechanism Design for Needle Translation

For translation of the three needle tubes, a compact, modular design was developed using specialty MRI compatible pneumatic cylinders (Airpot Airpel E9 Non-Magnetic). The concept for translation of the outermost tube is presented in Fig. 2. The piston rod is fixed to the front plate of the robot, which also serves as a needle guide. The needle tube is fixed to a sliding plate, which is supported by a pair of linear bearings and guide shafts. The cylinder is fixed to the sliding plate such that the movement of the cylinder, rather than the piston, provides actuation.

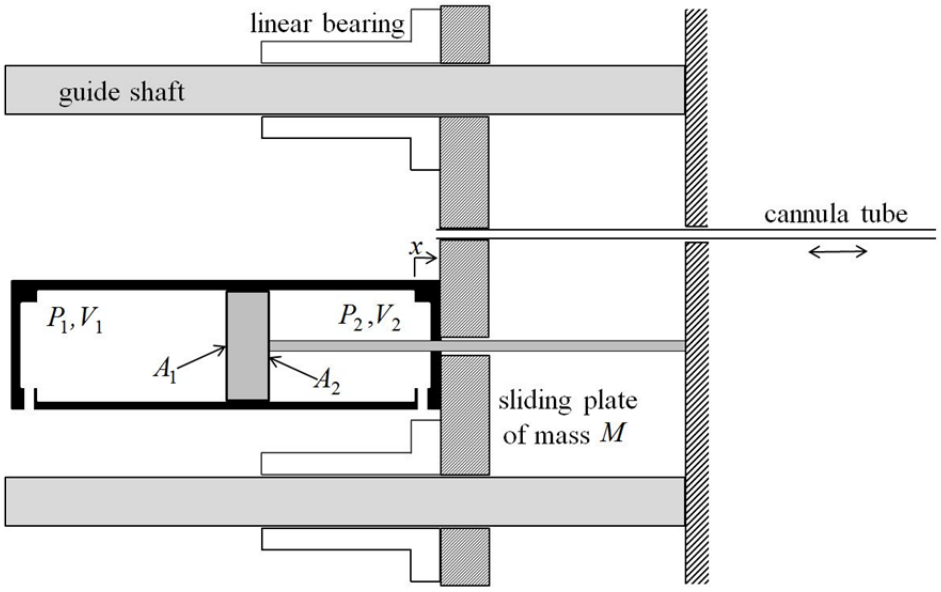

Figure 2: Sliding plate with piston-cylinder actuator to translate cannula tube

Similarly, two additional sliding plates translate the middle and innermost tubes. These translations are relative motions, because the piston rods are fixed to the first and the second sliding plates, respectively, as opposed to the stationary front plate with needle guide. The photograph of the robot in Fig. 3 shows the resulting mechanisms for needle tube translation.

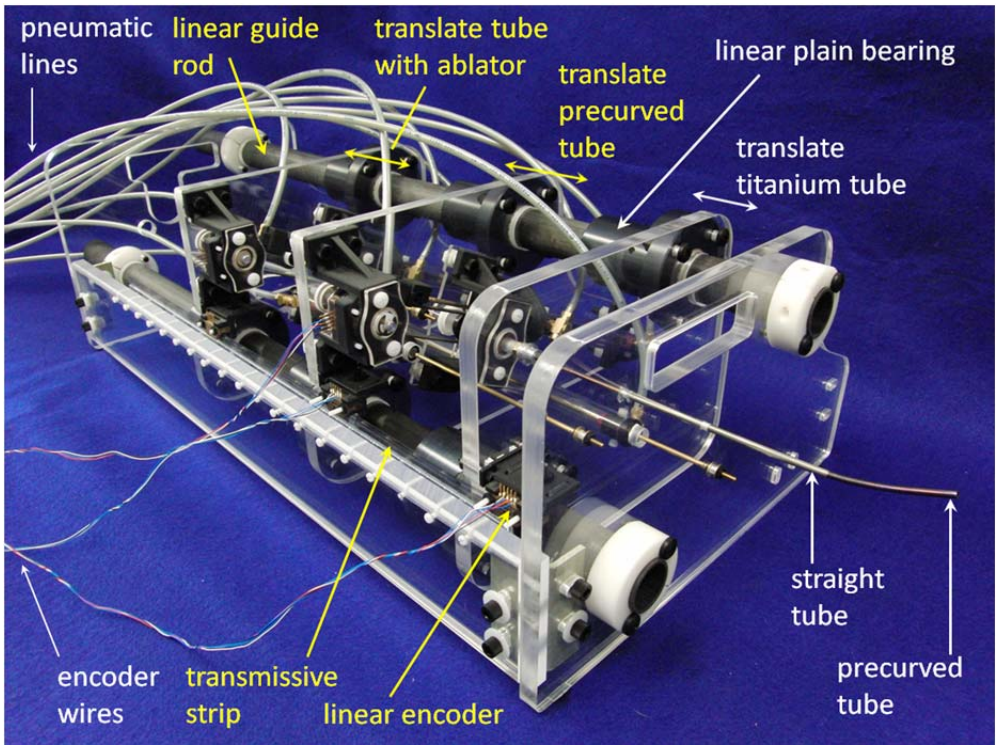

Figure 3: Photograph of five degree-of-freedom robot

2.2 Mechanism design for needle rotation

A low-friction, compact mechanism was needed to convert the linear motion of the actuator to rotation of the needle tubes. This transmission was designed to mount directly to the sliding plate, thus providing a modular design to both translate and rotate the needle tube. The tube clamps onto a hollow shaft, which is supported by a pair of ball bearings. The shaft and tube rotate when the piston and rod translate the linear portion of a timing belt. A photograph of one transmission on the robot is shown in Fig. 4.

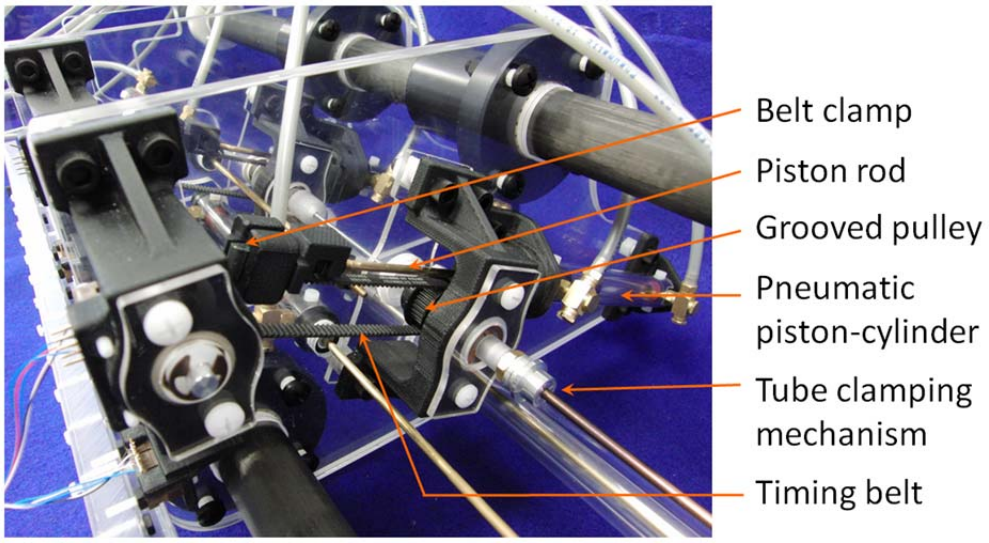

Figure 4: Transmission for rotary motion of needle tube

3 ROBOTIC SYSTEM DYNAMICS

The system dynamics for the robot include the equations of motion for the linear and rotary mechanisms as well as the gas dynamics for the piston-cylinders. For each actuator, a four-way spool valve controls the mass flow to both cylinder chambers.

3.1 Equation of Motion for the Sliding Plate

Using the quantities defined in Fig. 2, the equation of motion for each sliding plate is readily derived by Newton's Second Law. In Eq. 1, actuation force in the positive *x* direction corresponds to chamber 2 pressure P_2 and negative force corresponds to chamber 1 pressure P_1. Noting that the moving part of the actuator is the cylinder, not the piston, there are an additional two forces due to atmospheric pressure acting upon both ends of the cylinder. Finally, there is an unknown friction force F_f.

$$M\ddot{x} = P_2A_2 - P_1A_1 + P_{atm}A_1 - P_{atm}A_2 - F_f \tag{1}$$

Defining the piston rod cross-sectional area as $A_r = A_1 - A_2$, a simplified equation of motion is obtained. Anticipating that the robustness of the sliding mode controller can provide sufficient compensation for the unknown friction force, F_f is neglected, and the result is

$$M\ddot{x} = P_2A_2 - P_1A_1 + P_{atm}A_r \tag{2}$$

3.2 Equation of Motion for Tube Rotation Mechanism

A similar equation of motion for the linear-to-rotary mechanism can be derived. The mechanism behavior is more traditional in that the cylinder is stationary while the piston and

rod move. Thus, in keeping with the convention of P_2 denoting the rod-side pressure, the equation of motion is

$$M_{eff}\ddot{x} = P_1A_1 - P_2A_2 - P_{atm}A_r \tag{3}$$

where M_{eff} is the effective inertia of the piston, rod, timing belt, belt clamp, and rotating components. Again, the friction force has been neglected.

3.3 Actuator-Valve Dynamics

A four-way spool valve was selected to control the actuator. For this type of actuator-valve system, a thorough derivation of the gas dynamics model can be found in (8). These dynamics include the thermodynamics of the compressible gas in either cylinder chamber, as well as the mass flow through the valve orifice. Since a percutaneous intervention in the brain is a relatively slow-going operation, the required bandwidth for the robot is low. Therefore, the pressure dynamics are assumed to behave isothermally. From the mathematical model described in (8), the time derivative of each chamber pressure $\dot{P}_i$, $i = 1, 2$, is given for the isothermal case as

$$\dot{P}_i = \frac{RT}{V_i}\dot{m}_i - \frac{P_i\dot{V}_i}{V_i} \tag{4}$$

where R is the specific ideal gas constant and T is the ambient temperature. To provide a single input from the controller to the 4-way spool valve, the mass flows $\dot{m}_i$ into the chambers can be expressed as the product of valve orifice area A_v and area-normalized mass flow Ψ_i :

$$\begin{aligned} \dot{m}_1 &= -A_v\Psi_1(P_u, P_d) \\ \dot{m}_2 &= A_v\Psi_2(P_u, P_d) \end{aligned} \tag{5}$$

where the area-normalized mass flows are defined as

$$\Psi_1(P_u, P_d) = \begin{cases} \Psi(P_1, P_{atm}) & \text{for } A_v \geq 0 \\ \Psi(P_s, P_1) & \text{for } A_v < 0 \end{cases} \quad \text{and} \quad \Psi_2(P_u, P_d) = \begin{cases} \Psi(P_s, P_2) & \text{for } A_v \geq 0 \\ \Psi(P_2, P_{atm}) & \text{for } A_v < 0 \end{cases} \tag{6}$$

The area-normalized mass flow is a function of the pressures, P_u and P_d, upstream and downstream of the orifice, given in (9) as

$$\Psi(P_u, P_d) = \begin{cases} \dfrac{C_1C_fP_u}{\sqrt{T}} & \text{if } \dfrac{P_d}{P_u} \leq C_r \text{ (choked)} \\ \dfrac{C_2C_fP_u}{\sqrt{T}}\left(\dfrac{P_d}{P_u}\right)^{1/k}\sqrt{1-\left(\dfrac{P_d}{P_u}\right)^{(k-1)/k}} & \text{otherwise (unchoked)} \end{cases} \tag{7}$$

For the isothermal case, the temperature *T* of the flow is equal to ambient. The ratio of specific heats is $k = c_p / c_v$, and C_f is the dimensionless discharge coefficient dependent on valve orifice geometry. The pressure ratio C_r defines the flow as choked or unchoked, and the constants are given by

$$C_r = \left(\frac{2}{k+1} \right)^{\frac{k}{k-1}} \tag{8}$$

$$C_1 = \sqrt{\frac{k}{R}\left(\frac{2}{k+1} \right)^{(k+1)/(k-1)}} \text{ and } C_2 = \sqrt{\frac{2k}{R(k-1)}} \tag{9}$$

The gas dynamics are fully described by Eqs. 4 to 9 and relate the spool valve command to equation of motion given by Eq. 2. For control of the actuators and mechanisms described by Eq. 3, the sign of the valve command is opposite that which appears in Eq. 5, and thus the direction of mass flow is opposite of that in Eq. 6.

4 CONTROL DESIGN

A robust controller was required in order to handle the nonlinearity of the gas dynamics as well as the uncertainty of the friction force. Sliding mode control (SMC) is particularly well suited to provide robust control of nonlinear systems with unknown parameters. In prior work, sub-millimeter precision SMC control was achieved for the same type of MRI-compatible actuators now used on the 5-dof robot (6).

4.1 Control Law

A suitable SMC control law was formulated by choosing a third-order sliding surface acting on the integral of the position error:

$$s = \left(\frac{d}{dt} + \lambda \right)^3 \int e = \dddot{e} + 3\lambda \ddot{e} + 3\lambda^2 \dot{e} + \lambda^3 e \tag{10}$$

where $e = x - x_d$, x_d is the desired position, and λ is the desired closed-loop poles of the error dynamics. The system dynamics are third-order in position, as the affine control variable A_v appears by taking the time derivative of Eq. 2 and substituting in Eq. 4 to obtain

$$M \dddot{x} = A_2 \left(\frac{RT}{V_2} \ddot{m}_2 - \frac{P_2 \dot{V}_2}{V_2} \right) - A_1 \left(\frac{RT}{V_1} \ddot{m}_1 - \frac{P_1 \dot{V}_1}{V_1} \right) \tag{11}$$

To achieve stable error dynamics, the Lyapunov candidate function $V = \frac{1}{2} s^2$ was chosen, and its time derivative, $\dot{V} = s\dot{s}$, was set equal to a negative definite function of choice. The function $\dot{V}_{desired} = -\eta s \cdot \text{sat}(s)$ is a desirable choice because it forces the *s* dynamics to exhibit a smooth, exponential decay behavior:

$$\dot{s} = -\eta \,\mathrm{sat}(s) \tag{12}$$

where the saturation function $\mathrm{sat}(s)$ is bounded at ± 1, and η is the robustness constant of choice. The control law was obtained by taking the time derivative of Eq. 10, setting the result equal to Eq. 12, and substituting in Eq. 11. Solving the result for the command A_v:

$$A_v = \frac{\dddot{x}_d + f\left(P_i, V_i, \dot{x}\right) - 3\lambda\ddot{e} - 3\lambda^2\dot{e} - \lambda^3 e - \eta\,\mathrm{sat}(s)}{g\left(V_i, \Psi_i\right)} \tag{13}$$

where the functions *f* and *g* are given by

$$f\left(P_i, V_i, \dot{x}\right) = \frac{1}{M}\left(A_1^2\frac{P_1}{V_1} + A_2^2\frac{P_2}{V_2}\right)\dot{x} \tag{14}$$

$$g\left(V_i, \Psi_i\right) = \frac{RT}{M}\left(\frac{A_1}{V_1}\Psi_1 + \frac{A_2}{V_2}\Psi_2\right) \tag{15}$$

In Eq. 14, velocity has been introduced by noting that $\dot{V}_1 = -A_1\dot{x}$ and $\dot{V}_2 = A_2\dot{x}$. The control law provides a Lyapunov-stable closed-loop error dynamics for the sliding mode controller.

4.2 Control Electronics and Settings

To make the electronics MRI-compatible, five optical encoders were used for sensing linear and rotary positions of the actuators. A linear transmissive strip with 197 lines per cm (500 lines per inch) is used with three linear encoders to sense position of the three sliding plates. Two rotary encoders with 1250 counts per revolution provide angular position of the needle tubes. The encoders provided a clean signal that was digitally differentiated to provide velocity and acceleration, with second-order low pass filters at 100 Hz. For each actuator, additional electronics were one Festo 4-way spool valve and two 0-16 bar Festo pressure sensors to measure both chamber pressures.

Control accuracy was also improved through careful measurement of three dead volumes in the system: the pressure sensor with its fitting and the entry ports to each of the two cylinder chambers, with their fittings. Measurements were obtained using a syringe with 0.01 mL increments and isopropyl alcohol. This fluid has a low surface tension and thus it provided an accurate measurement because very few air bubbles were formed.

5 RESULTS

The controller was tested on the robot with the needle moving in free space. Position tracking of the sliding plate is shown in Fig. 5, where the reference signal is a 0.25 Hz square wave of 30 mm peak-to-peak amplitude. For this test the supply pressure of 310 kPa gage (45 psi) was capable of producing a maximum force of 21.0 N (4.72 lbf). The mean steady-state error was 6 microns, which is one half the resolution of the linear encoder when

it is read in quadrature. Shown in Fig. 6, the steady-state error appears to be less than the encoder resolution, but this is simply because the reference position is not an exact multiple of the encoder counts. Optimal values for the control parameters were $\lambda = 20$ Hz and $\eta = 2$ m^3/sec.

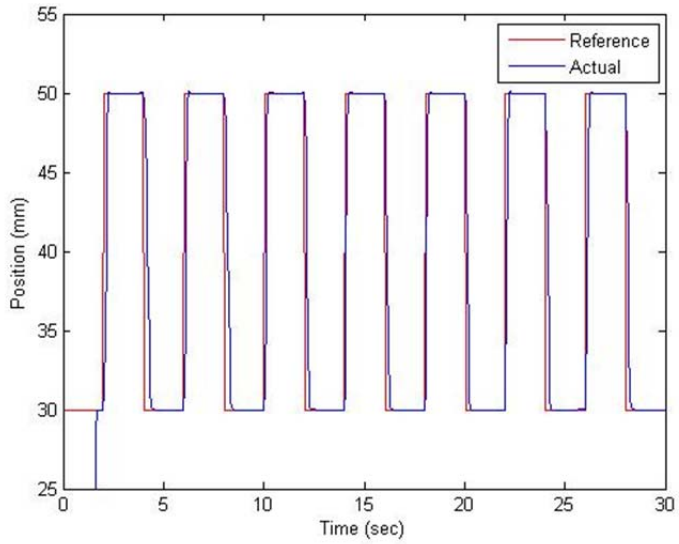

Figure 5: Position tracking for translation of sliding plate

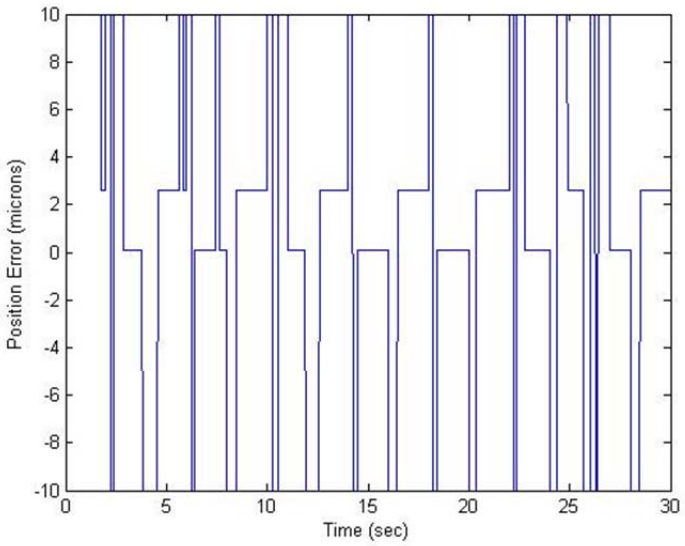

Figure 6: Steady-state position error for translation of sliding plate

Similarly, controller performance for rotation of the needle tube is shown in Figs. 7 and 8. The reference was a 0.25 Hz square wave with peak-to-peak amplitude of 120 degrees. The controller achieved a mean steady-state error of 0.3 degrees with the control parameters tuned to $\lambda = 15$ Hz and $\eta = 2$ m^3/sec.

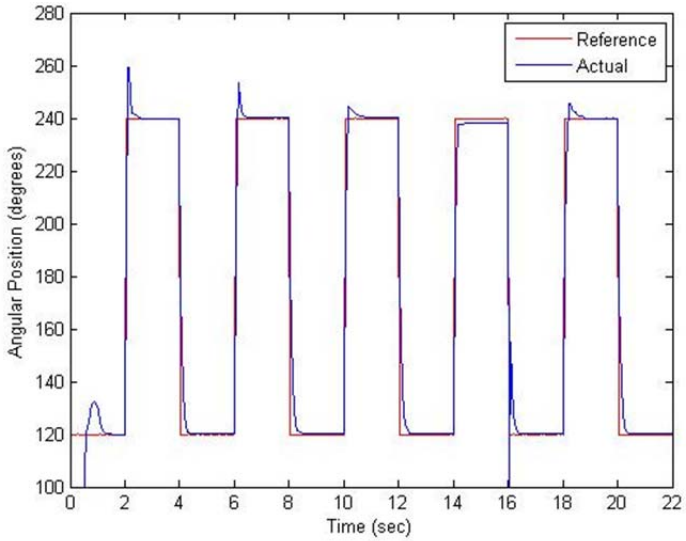

Figure 7: Angular position tracking for rotation of needle tube

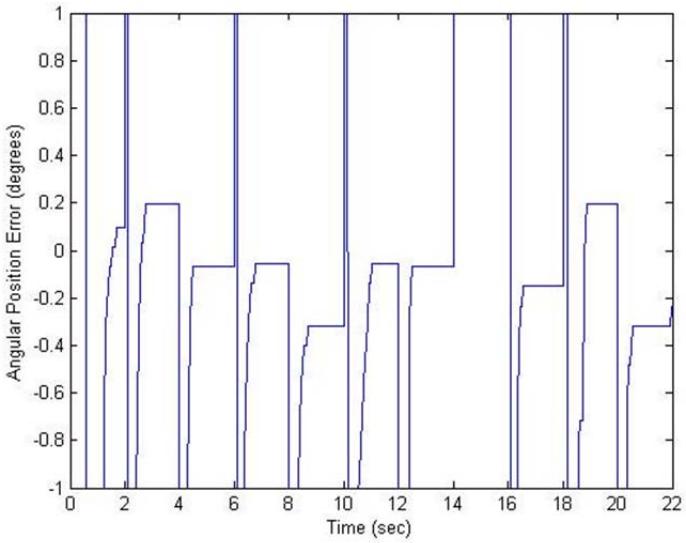

Figure 8: Steady-state angular position error for rotation of needle tube

5 CONCLUSION

An ideal solution for MRI-compatible robots, pneumatic actuators can easily integrate with the nitrogen or instrument air supply in hospitals. As the supply is sterile and inert, leakage is not a safety concern. Furthermore, pneumatic actuators do not reduce the scanner SNR. In light of these advantages, a 5-dof robot was designed and built to steer an active cannula by pneumatic actuation. The robot provides both translation and rotation to needle tubes by a modular design, such that additional tubes could easily be added to the cannula. Thus, while the robot was originally designed for a specific clinical application, the design could easily be modified for treatment of tumors or other disorders in the brain.

Using sliding mode control, high accuracy position tracking has been achieved for both the translation and rotation actuators. Since typical MRI resolutions are 1 mm, the reported accuracy of the controller suggests the robot has the potential to produce excellent results for needle tip targeting experiments, which will be conducted in future research.

REFERENCES

(1) Kwan, P. and Brodie, M. J., 2000, "Early Identification of Refractory Epilepsy," *N Engl J Med*, **342**(5), pp. 314-319.

(2) de Flon, P., Kumlien, E., Reuterwall, C., and Mattsson, P., 2010, "Empirical Evidence of Underutilization of Referrals for Epilepsy Surgery Evaluation," *European Journal of Neurology*, **17**, pp. 619-625.

(3) Engel, J., Jr., Wiebe, S., French, J., Sperling, M., Williamson, P., Spencer, D., Gumnit, R., Zahn, C., Westbrook, E., and Enos, B., 2003, "Practice Parameter: Temporal Lobe and Localized Neocortical Resections for Epilepsy," *Epilepsia*, **44**(6), pp. 741-751.

(4) Lhatoo, S. D., Solomon, J. K., McEvoy, A. W., Kitchen, N. D., Shorvon, S. D., and Sander, J. W., 2003, "A Prospective Study of the Requirement for and the Provision of Epilepsy Surgery in the United Kingdom," *Epilepsia*, **44**(5), pp. 673-676.

(5) Fischer, G. S., Krieger, A., Iordachita, I., Csoma, C., Whitcomb, L. L., and Fichtinger, G., 2008, "MRI Compatibility of Robot Actuation Techniques – A Comparative Study," *Int Conf Medical Image Computing and Computer Assisted Intervention*, New York, NY, **5242**, pp. 509-517.

(6) Comber, D. B. and Barth, E. J., 2011, "Precision Position Tracking of MR-Compatible Pneumatic Piston-Cylinder Using Sliding Mode Control," DSCC2011-5960, *Proc. DSCC & Bath/ASME Symp. Fluid Power and Motion Control*, Arlington, VA, pp. 1-7.

(7) Fischer, G., Iordachita, I., Csoma, C., Tokuda, J., DiMaio, S., Tempany, C., Hata, N., and Fichtinger, G., 2008, "MRI-Compatible Pneumatic Robot for Transperineal Prostate Needle Placement," *IEEE/ASME Trans. Mechatronics*, **13**(3), pp. 295-305.

(8) Richer, E. and Hurmuzlu, Y., 2000, "A High Performance Pneumatic Force Actuator System: Part 1—Nonlinear Mathematical Model," *ASME J. Dyn. Syst., Meas. Control*, **122**(3), pp. 416-425.

(9) Ben-Dov, D., and Salcudean, S., 1995, "A Force-Controlled Pneumatic Actuator," *IEEE Trans. Robotics & Automation*, **11**(6), pp. 906-911